# Distributed Volt/VAr Control by PV Inverters

Pedram Jahangiri, *Student Member, IEEE*, and Dionysios C. Aliprantis, *Senior Member, IEEE*

***Abstract*—A major technical obstacle for rooftop photovoltaics (PV) integration into existing distribution systems is the voltage rise due to the reverse power flow from the distributed PV sources. This paper describes the implementation of a voltage control loop within PV inverters that maintains the voltage within acceptable bounds by absorbing or supplying reactive power. In principle, this can be considered to be a form of distributed Volt/VAr control, which is conventionally performed by coordinated control of capacitor banks and transformer tap changers. Comprehensive simulation studies on detailed feeder models are used to demonstrate that the proposed control scheme will mitigate voltage rises.**

***Index Terms*—Photovoltaic power systems, power distribution, reactive power control, voltage control.**

## I. Introduction

THE installed capacity of embedded rooftop photovoltaic (PV) generation in residential distribution systems is rising rapidly worldwide [1], driven by reductions in costs, increases in electricity prices, and higher sensitivity about sustainability. Under the premise that this exponential trend will continue unabated, power distribution utilities must ensure that the quality of service to their customers will not be compromised [2], [3]. For instance, the increased penetration of distributed PV sources has been cause of concern for harmonic pollution, but this issue can be resolved with standardization regarding harmonic distortion limits and the use of appropriate power electronic topologies.

A major obstacle for further PV integration into existing medium/low-voltage networks is the induced voltage rise due to the reverse power flow along the distribution feeders [4]–[10]. This phenomenon is bound to be exacerbated under higher penetration of PV sources. In the United States, the ANSI Standard C84.1 [11] states that the voltage of residential loads should remain within five percent from its nominal value (120 V) under normal operating conditions.

Several techniques to alleviate the voltage rise issue have been proposed. These can be employed by the utility itself or by its customer-owners of distributed PV generation (in this case, either appropriate financial incentives or regulation might be necessary). One simple solution is to lower the setpoint of the on-load tap changer at the high-voltage/medium-voltage substation, or to use a voltage regulator [12]. However, this method cannot guarantee that the voltage profile will be within acceptable bounds throughout the feeder. In addition, other feeders that might be connected to the same transformer may be adversely impacted by this action [4]. Alternatively, the utility can choose to reinforce the distribution grid, by increasing conductor sizes to reduce the resistance of medium- and low-voltage lines. In Germany, where installed capacity of PV systems increased at a much faster rate than the development of new controllers or the updating of grid codes, this practice has led to high costs [4], [9]. Yet another solution is to curtail real power feed-in from PV units at times of low demand. For instance, in the Japanese grid code, when the voltage at the point of common coupling exceeds the upper limit, the PV system is required to reduce its active power output [7], [9], [13]–[15]. The disadvantage of this technique is that it causes the spilling of solar energy, which is not economically attractive to the PV panel owners.

The approach considered herein is to absorb reactive power using the PV inverters themselves, in a distributed fashion.[1] This is feasible even though the X/R ratio in distribution systems is typically smaller than in transmission systems and therefore, reactive power has a relatively lower impact on voltage magnitude. Nevertheless, as will be demonstrated in this paper as well, appropriate reactive power control can offset the voltage rise in distribution networks, while reducing or deferring the need for new assets or grid reinforcements [7]–[9], [14], [17].

This study considers the implementation of a voltage control loop within rooftop PV inverters, to maintain the voltage within acceptable bounds by reactive power injection or absorption. In principle, this can be considered to be a form of Volt/VAr control, which is conventionally performed by coordinated control of capacitor banks located along the feeder and transformer tap changers. In the proposed implementation, the voltage control objective is accomplished with a piecewise linear droop characteristic, which determines the reactive power injection as a function of the voltage magnitude at the PV inverter terminals. This control strategy has been studied in [6], [8], [18], [19], and by other researchers. Notably, the control is simple to implement, and does not require communication or cooperation among the PV inverters [14], [20].

The main objective of this analysis is to provide evidence through comprehensive simulation studies that this control scheme will mitigate voltage rise, at essentially no extra investment cost to the consumer. In all cases that were analyzed, voltage violations were completely eliminated. Previous work on this topic is extended in the following ways: 1) Studies are performed by means of computer simulations of several realistic distribution feeders with hundreds of households and their appliances modeled in high detail. To our knowledge, this is the first time that this type of controller is demonstrated with

Manuscript received October 03, 2012; revised March 05, 2013; accepted March 29, 2013. Date of publication April 25, 2013; date of current version July 18, 2013. This material is based upon work supported by the Electric Power Research Center of Iowa State University. Paper no. TPWRS-01111-2012.

The authors are with the Department of Electrical and Computer Engineering, Iowa State University, Ames, IA 50011 USA (e-mail: pedramj@iastate.edu; dali@iastate.edu).

Digital Object Identifier 10.1109/TPWRS.2013.2256375

[1]Controlling real and reactive power output implies that PV units actively participate in grid voltage control. The grid codes of some countries, such as the United States (based on the IEEE Standard 1547 series), prohibit active voltage regulation of PV units at the point of common coupling [9]. Deliberations to relieve this constraint are under way, in light of new technologies and emerging higher penetrations of distributed energy resources [16].

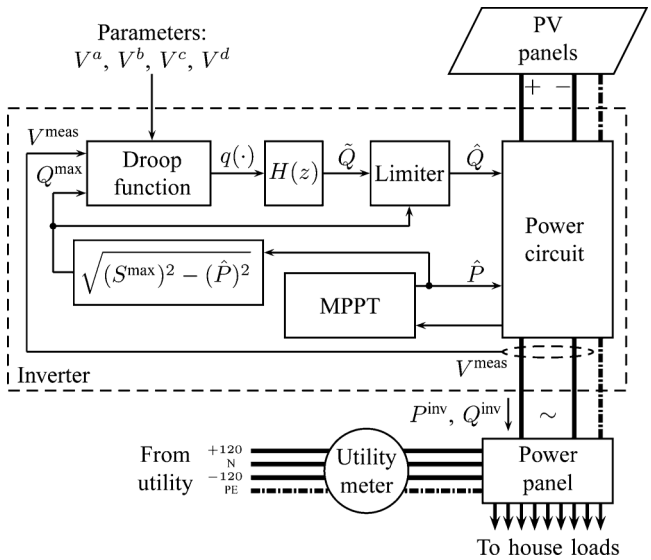


Fig. 1. Block diagram of a PV inverter with voltage controller (for a United States-based system).

such degree of modeling verisimilitude, since past work has used feeder models of limited size and fidelity. The simulations are run using GridLAB-D [21], which is an open-source software platform developed by the U.S. Department of Energy at the Pacific Northwest National Laboratory (PNNL) for the simulation of electric power distribution systems. GridLAB-D has a comprehensive library of precise load models, including their dependence on voltage levels. The original inverter source code of GridLAB-D was modified to represent the proposed control. 2) The dynamic interactions between a large number of inverters operating in tandem are taken into account. In particular, a transfer function that helps stabilize the system by eliminating unwanted oscillatory (hunting) behavior is introduced in the control path. This phenomenon has not been previously mentioned in the PV literature, but it was revealed by our simulations. 3) The reactive power capability of the inverter is modeled accurately, as dynamically dependent on the real power generation. This is important because during times of peak PV power generation, reactive power generation capability is limited the most, exactly when it is most needed by the system. 4) The inverter losses are accounted for with a simple model. 5) The cumulative side-effects of the proposed scheme at the substation are observed.

The remainder of this paper is organized as follows. Section II sets forth the proposed controller and discusses its stability. Illustrative findings from computer simulations are reported in Section III. Concluding remarks are provided in Section IV. In the Appendices, the reader may find system parameters and comprehensive tabulated results from the simulation studies.

## II. Control Strategy

This section discusses the envisioned practical implementation of the proposed voltage controller as a discrete-time dynamic system, including its stability properties. Fig. 1 shows the proposed modification to an otherwise standard PV inverter with maximum power point tracking (MPPT) functionality.

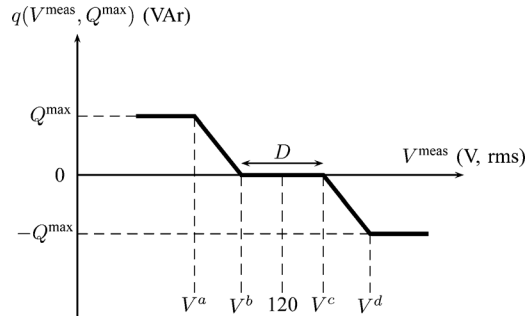


Fig. 2. Droop control function (for a United States-based system).

### A. Reactive Power Support Function

The MPPT algorithm determines the desired real power output at each period $n$, $\hat{P}_n$, whereas the actual output accounts for the loss in the inverter, $P_n^{\text{inv}} = \hat{P}_n - P_{\text{loss},n}$. The desired reactive power output $\hat{Q}_n$ is determined by the proposed controller using the function $q(V^{\text{meas}}, Q^{\max})$, which is depicted in Fig. 2. The actual reactive power output is $Q_n^{\text{inv}} \approx \hat{Q}_n$. The reactive power compensation loop could be automatically turned off overnight since under normal conditions, feeders operate within the acceptable voltage range in the absence of PV generation. Of course, the controller would have other functions that are not shown here, such as a phase-locked loop for tracking the terminal voltage and anti-islanding detection schemes. The generation of an additional reactive power component is relatively simple to implement (for example, using $qd$ reference frame theory), and amounts to injecting the appropriate current component ninety degrees out of phase with the voltage.

The droop characteristic is a piecewise linear function of the voltage. It is dynamically changing due to its dependence on the maximum reactive power capability, $Q^{\max}$, which in turn depends on the variable real power output of the inverter. In general, the droop characteristic can be defined in terms of four parameters, $V^a$, $V^b$, $V^c$, and $V^d$, or by three parameters $V^a$, $D$ (deadband width), and $V^d$, if the deadband is symmetric around the nominal voltage value. These parameters can be hard-coded, or programmed at the time of installation by a technician (according to the recommendations of the distribution system utility). It is also conceivable in a future "smart grid" scenario that these parameters could be dynamically adjusted by the distribution system operator via a communications network, which opens interesting opportunities for system performance optimization on a regular basis, for instance, as seasons and load patterns change, or if the feeder topology is modified (e.g., due to feeder growth).

The maximum reactive power capability of the inverter at period $n$, which essentially reflects a current limitation, is defined by

$$Q_n^{\max} = \sqrt{(S^{\max})^2 - (\hat{P}_n)^2}. \tag{1}$$

This is recomputed at every period based on the real power generation and the apparent power rating of the inverter $S^{\max}$. Inside the deadband, $q(\cdot) = 0$ since the voltage is close to its nominal value. When the measured voltage exceeds $V^c$, the converter starts absorbing reactive power, in a bid to lower the voltage. At $V^d$ and beyond, the inverter is asked to absorb the maximum possible reactive power. This is the most common

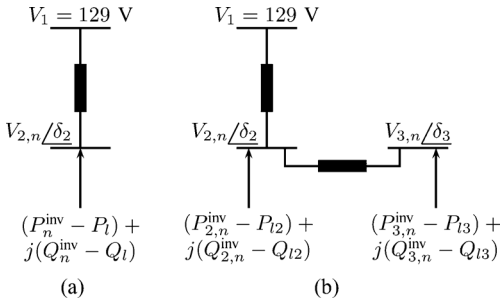


Fig. 3. Two-bus and three-bus system examples.

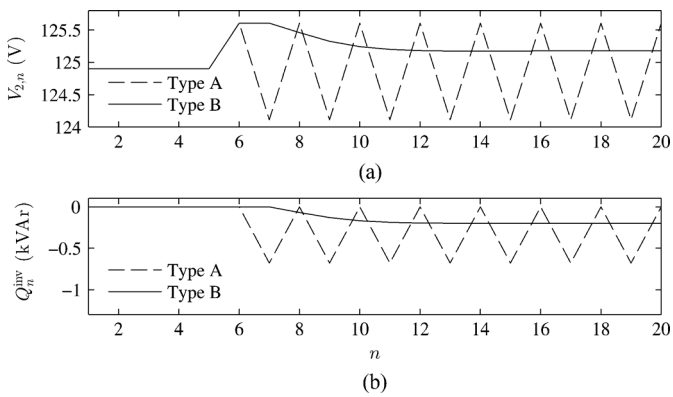


Fig. 4. Two-bus system: voltage magnitudes and reactive power injections from PV inverter.

operating mode, due to the voltage rise phenomenon by PV generation. Nevertheless, this controller can also contribute to the mitigation of low-voltage occurrences, e.g., for locations far away from the substation under heavy load conditions, when the voltage drops below $V^b$.

It is interesting to note that the $q(\cdot)$ characteristic does not have to be symmetric. In fact, variations of this function have been proposed in the past. For instance, a "transmission VAr support" mode has been proposed [16], where the PV inverter will not absorb reactive power for voltages higher than $V^b$, if signaled to do so by the utility. Another modification would be to use constant slope (rather than a dynamically changing one) below $V^b$ and above $V^c$, until $\pm Q^{\max}$ is reached. The constant slope method could be interesting from a theoretical standpoint, since one could relate this slope to the Jacobian of the power flow, and possibly determine its optimal value analytically. However, such study is left for future work. Yet another example would be the necessary modification of the characteristic for utilities adopting a Conservation Voltage Reduction scheme [22], where an asymmetric function might be desirable. In addition, in cases where the reactive power control scheme fails to regulate voltages within acceptable bounds, then an outer loop that would curtail PV real power production could be activated. In any case, all studies performed here utilize the "canonical" droop characteristic of Fig. 2.

If the PV system uses a central inverter, which is typically installed in close proximity to the main power panel, then the voltage at its terminals would be approximately equal to the voltage at the point of interconnection with the utility. Some newer PV systems use micro-inverters, embedded into the panels themselves, in which case the control scheme should be modified to account for the voltage drop in the wires connecting the inverters to the power panel. Alternatively, it is conceivable that an advanced meter might have the capability to communicate its voltage measurement to the inverters via a home area network, as proposed in [18]. In our implementation, central inverters are considered, and they are assumed to be wired to the 240 V, rms[2] coming from a center-tapped distribution transformer. (A division of the measured voltage by a factor of two takes place in the control loop.)

### B. Instability Concerns

A simple digital implementation of the control scheme shown in Fig. 1 can be modeled as a discrete-time system with a "Type-A" transfer function $H_A(z) = z^{-1}$. It was observed that this led to an undesirable oscillatory behavior. To mitigate this, a "Type-B" transfer function, whose response resembles that of a continuous-time transfer function of the form $1/(1+\tau s)$, is defined by

$$H_B(z) = \frac{1}{\left(1 - \frac{\tau}{\Delta T}\right) + \left(\frac{\tau}{\Delta T}\right) z}. \tag{2}$$

Hence, the discrete-time response can be expressed as

$$\tilde{Q}_{n+1} = \begin{cases} q(V_n^{\text{meas}}, Q_n^{\max}) & \text{for Type-A systems} \\ \left(1 - \frac{\Delta T}{\tau}\right) \tilde{Q}_n + \left(\frac{\Delta T}{\tau}\right) q(V_n^{\text{meas}}, Q_n^{\max}) & \text{for Type-B systems.} \end{cases} \tag{3}$$

Here, the sampling time is $\Delta T = 1$ s, and the time constant is $\tau = 10$ s.

In order to demonstrate the potential instability of the simple control scheme that uses the Type-A transfer function, two simple examples have been devised, illustrated in Fig. 3, with parameters provided in Appendix A. The reader may refer to Section II-C for a theoretical analysis of system stability.

First, consider the hypothetical two-bus single-phase system of Fig. 3(a). Bus 1 is the slack bus and bus 2 is a load (PQ) bus with a PV system.[3] Initially, the PV system is generating zero real power, and since the voltage of bus 2 (124.90 V) is inside the deadband, the inverter is not injecting reactive power. During period 6, the real power generation is stepped from 0 to 1 kW, which causes the voltage to rise, and an oscillation to begin as the inverter tries to mitigate this. As can be observed from Fig. 4(a), the voltage at bus 2 is oscillating between 125.61 V and 124.11 V, with the corresponding reactive power injections shown in Fig. 4(b). Fig. 4(a) also illustrates the response when the controller includes the Type-B transfer function. Now the oscillations are damped and the system reaches a stable operating point ($V_2 = 125.18$ V, $Q^{\text{inv}} = -197.32$ VAr).

The second example (see Fig. 3(b)) demonstrates the potential instability caused by two inverters interacting with each

[2]All voltages in the paper are provided as rms values.

[3]The commonly used notation for synchronous generator buses in standard power flow formulations, where real power and voltage are given, and which are thus termed "PV" buses, conflicts with the abbreviation of the word "photovoltaic." It is important to stress that photovoltaic inverters are *not* modeled as PV buses, but as PQ buses, where real and reactive power output change in every period $n$. Hence, the analysis is based on a sequence of quasi-steady-state power flow solutions.

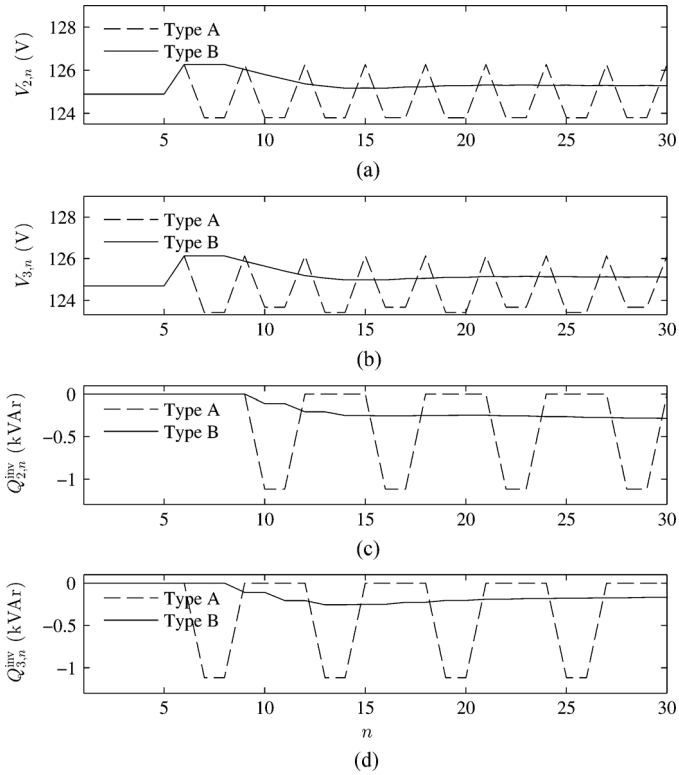


Fig. 5. Three-bus system: (a) and (b) voltage magnitudes; (c) and (d) reactive power injections from PV inverters.

other when their control schemes use the type-A transfer function. In practice, the two inverters will not be necessarily acting in a synchronized manner, so here they are evenly staggered for simplicity: the bus-2 inverter acts in odd periods, whereas the bus-3 inverter acts in even periods. Initially, the PV systems are not generating real power, and since the voltages of bus 2 and bus 3 are inside the deadband ($V_2 = 124.90$ V, $V_3 = 124.69$ V), their inverters are not injecting reactive power. During period 6, the real power generation of both inverters is stepped from 0 to 1 kW, which causes the voltages to rise, and oscillations to begin as the inverters try to mitigate them. As can be observed from Fig. 5(a) and (b), the voltages at buses 2 and 3 are oscillating, with corresponding reactive power injections shown in Fig. 5(c) and (d). The response of the system when the Type-B transfer function is used is superimposed in Fig. 5. Now the oscillations are damped and the system reaches a stable operating point ($V_2 = 125.28$ V, $Q_2^{\text{inv}} = -318.16$ VAr, $V_3 = 125.12$ V, $Q_3^{\text{inv}} = -132.82$ VAr).

Similar oscillations have been observed in the simulations of the realistic feeders described in the next section. However, due to space limitations, such results are not shown here. Using the Type-B transfer function eliminated this type of hunting behavior in all cases. A more general framework for stability analysis of these types of systems is established in the next subsection.

### C. Stability Analysis

Consider the general case of an $N$-bus distribution feeder system with a constant-voltage slack bus representing the substation, and $N-1$ load buses with PV inverters, i.e., $N-1$ PQ buses. For simplicity, let this be a single-phase system, and let all inverters act in a synchronized manner. (The analysis can be extended to the general case of a three-phase unbalanced feeder with staggered inverter actions, but this will be unnecessarily complicated, and will distract the reader from the main purpose of this section, which is to illustrate why the system is inherently unstable and how it is stabilized.) Assume that the real power output of each inverter remains constant, so that the droop characteristic only depends on the measured voltage. Voltage measurement errors are neglected. Also assume that the limiter blocks are not activated, i.e., $\hat{Q} = \tilde{Q}$, and that the reactive power output of the inverter is equal to the commanded value, i.e., $Q^{\text{inv}} = \hat{Q}$.

This dynamic system has $N-1$ states representing the reactive power output of each inverter during period $n$, contained in a column vector $\hat{Q}_n = [\hat{Q}_{2,n}\ \hat{Q}_{3,n}\ \cdots\ \hat{Q}_{N,n}]^T$. The state equation is

$$\hat{Q}_{n+1} = f(\hat{Q}_n) = \begin{cases} q(V(\hat{Q}_n)) & \text{for Type-A systems} \\ \left(1 - \frac{\Delta T}{\tau}\right)\hat{Q}_n + \left(\frac{\Delta T}{\tau}\right) q(V(\hat{Q}_n)) & \text{for Type-B systems.} \end{cases} \tag{4}$$

The vector $q(V(\hat{Q}_n)) = [q_2(V_2(\hat{Q}_n))\ \cdots\ q_N(V_N(\hat{Q}_n))]^T$ contains the droop control function outputs of each inverter as functions of the local bus voltages. These voltages are in turn related to the reactive power injections of all inverters through the power flow equations of the network. It can be readily shown that both Type-A and Type-B system stationary states (or fixed points) $\bar{Q} = [\bar{Q}_2\ \bar{Q}_3\ \cdots\ \bar{Q}_N]^T$ satisfy the nonlinear equation:

$$\bar{Q} = f(\bar{Q}) = q(V(\bar{Q})). \tag{5}$$

The stability of a nonlinear discrete-time system in the vicinity of its stationary states can be determined using the following theorem [23]:

*Theorem:* For the discrete-time system $X_{n+1} = \phi(X_n)$, suppose $\phi : \mathbb{U} \to \mathbb{U}, \mathbb{U} \subseteq \mathbb{R}^m$, is continuously differentiable in some neighborhood of a fixed point $\bar{X} \in \mathbb{U}$. Let $J = [\partial\phi/\partial X]_{X=\bar{X}}$ be the Jacobian matrix of $\phi$, evaluated at $\bar{X}$. Then:

- $\bar{X}$ is asymptotically stable if all eigenvalues of $J$ have magnitude less than 1.
- $\bar{X}$ is unstable if at least one eigenvalue of $J$ has magnitude greater than 1.

In our application, the Jacobian matrix of (4) becomes

$$J = \left[\frac{\partial f}{\partial \hat{Q}}\right]_{\hat{Q}=\bar{Q}} = \begin{cases} \left[\frac{\partial q}{\partial V}\right]\left[\frac{\partial V}{\partial \hat{Q}}\right] & \text{for Type-A systems} \\ \left(1 - \frac{\Delta T}{\tau}\right)\mathbb{I} + \left(\frac{\Delta T}{\tau}\right)\left[\frac{\partial q}{\partial V}\right]\left[\frac{\partial V}{\partial \hat{Q}}\right] & \text{for Type-B systems} \end{cases} \tag{6}$$

where $[\partial q/\partial V]$ is a diagonal matrix:

$$\left[\frac{\partial q}{\partial V}\right] = \begin{bmatrix} \frac{\partial q_2}{\partial V_2} & & 0 \\ & \ddots & \\ 0 & & \frac{\partial q_N}{\partial V_N} \end{bmatrix}. \tag{7}$$

The diagonal elements represent the slopes of the individual droop control functions. They can have zero or negative value,

depending on the segment in which the stationary point happens to be located.[4] The matrix $[\partial V/\partial \hat{Q}]$ contains the partial derivatives:

$$\left[\frac{\partial V}{\partial \hat{Q}}\right] = \begin{bmatrix} \frac{\partial V_2}{\partial \hat{Q}_2} & \frac{\partial V_2}{\partial \hat{Q}_3} & \cdots & \frac{\partial V_2}{\partial \hat{Q}_N} \\ \frac{\partial V_3}{\partial \hat{Q}_2} & \frac{\partial V_3}{\partial \hat{Q}_3} & \cdots & \frac{\partial V_3}{\partial \hat{Q}_N} \\ \vdots & \vdots & & \vdots \\ \frac{\partial V_N}{\partial \hat{Q}_2} & \frac{\partial V_N}{\partial \hat{Q}_3} & \cdots & \frac{\partial V_N}{\partial \hat{Q}_N} \end{bmatrix}. \tag{8}$$

Define $A = [\partial q/\partial V][\partial V/\partial \hat{Q}]$, and let an eigenvalue of the Type-A Jacobian matrix be denoted by $\lambda$, satisfying $Ax = \lambda x$. From the Type-B expression of (6), we have

$$\begin{aligned} &\left[\left(1-\frac{\Delta T}{\tau}\right)\mathbb{I} + \left(\frac{\Delta T}{\tau}\right)A\right]x \\ &\quad = \left(1-\frac{\Delta T}{\tau}\right)x + \left(\frac{\Delta T}{\tau}\right)Ax \\ &\quad = \left[\left(1-\frac{\Delta T}{\tau}\right) + \left(\frac{\Delta T}{\tau}\right)\lambda\right]x\,. \end{aligned} \tag{9}$$

This implies that the corresponding eigenvalue of the Type-B Jacobian matrix will be

$$\mu = \left(1-\frac{\Delta T}{\tau}\right) + \left(\frac{\Delta T}{\tau}\right)\lambda\,. \tag{10}$$

For example, if $\Delta T = 1$ s, and $\tau = 10$ s, then $\mu = 0.9 + 0.1\lambda$.

It is interesting to note what happens if the stationary point of the inverter on bus $i$ lies on the flat region of the droop characteristic. In this case, the corresponding $\partial q_i/\partial V_i$ term is equal to zero. This, in turn, implies that row $(i-1)$ of the Jacobian $J$ will be zero for Type-A systems, or that it will only contain a $(1-\Delta T/\tau)$ element in the diagonal for Type-B systems. The former case leads to a zero eigenvalue; the latter case leads to an eigenvalue of the same value as the element itself. In both cases, the corresponding eigenvalue is a real number less than one, hence stability is not adversely affected.

To calculate $[\partial V/\partial \hat{Q}]$, we first write the power flow equations as implicit functions of the reactive power injections by the PV inverters $\hat{Q}$:

$$P(\delta(\hat{Q}), V(\hat{Q})) - (P^{\text{inv}} - P_l) = 0 \tag{11}$$

$$Q(\delta(\hat{Q}), V(\hat{Q})) - (\hat{Q} - Q_l) = 0. \tag{12}$$

Here, the vector functions $P = [P_2\ P_3\ \ldots\ P_N]^T$ and $Q = [Q_2\ Q_3\ \ldots\ Q_N]^T$ represent real and reactive power injections, respectively. The other variables, $P^{\text{inv}}$, $P_l$, and $Q_l$, are constant vectors. The power injections at each load bus, $P_i$ and $Q_i$, $i = 2, 3, \ldots, N$, are given by

$$P_i = \sum_{j=1}^{N} V_i V_j |Y_{i,j}| \cos(\delta_j - \delta_i + \theta_{i,j}) \tag{13}$$

$$Q_i = -\sum_{j=1}^{N} V_i V_j |Y_{i,j}| \sin(\delta_j - \delta_i + \theta_{i,j}) \tag{14}$$

[4]Application of the theorem to the special case where the stationary point happens to be exactly on a corner point of the droop characteristic ($V^a$, $V^b$, $V^c$, or $V^d$) is problematic, since the function $f$ is not differentiable. However, this issue can be readily resolved by adding a slight curvature to $q(\cdot)$ around these points.

where the elements of the nodal admittance matrix of the system are denoted by $Y_{i,j} = |Y_{i,j}|\underline{/\theta_{i,j}}$. Hence, from (11)–(12), we obtain

$$\left[\frac{\partial P}{\partial \hat{Q}}\right] = \left[\frac{\partial P}{\partial \delta}\right]\left[\frac{\partial \delta}{\partial \hat{Q}}\right] + \left[\frac{\partial P}{\partial V}\right]\left[\frac{\partial V}{\partial \hat{Q}}\right] = 0 \tag{15}$$

$$\left[\frac{\partial Q}{\partial \hat{Q}}\right] = \left[\frac{\partial Q}{\partial \delta}\right]\left[\frac{\partial \delta}{\partial \hat{Q}}\right] + \left[\frac{\partial Q}{\partial V}\right]\left[\frac{\partial V}{\partial \hat{Q}}\right] = \mathbb{I}. \tag{16}$$

Manipulation of (15)–(16) yields

$$\left[\frac{\partial V}{\partial \hat{Q}}\right] = \left\{\left[\frac{\partial Q}{\partial V}\right] - \left[\frac{\partial Q}{\partial \delta}\right]\left[\frac{\partial P}{\partial \delta}\right]^{-1}\left[\frac{\partial P}{\partial V}\right]\right\}^{-1}. \tag{17}$$

This expression is based on the four submatrices of the Jacobian of the power flow problem (not to be confused with the Jacobian of the dynamic system function $f$), which have well-known expressions that can be computed from (11)–(12) or found in a power systems textbook.

This analysis is illustrated using the two simple systems that were introduced in the previous section.

*1) Stability of Two-Bus Example:* The two-bus system example is a one-dimensional discrete-time system. Its stationary state is $\bar{Q}_2 = -197.32$ VAr. This point corresponds to the fourth segment of the droop control function (between $V^c$ and $V^d$), which implies that

$$\frac{\partial q_2}{\partial V_2} = \frac{-Q^{\max}}{V^d - V^c} = -1118\ \frac{\text{VAr}}{\text{V}}. \tag{18}$$

The power flow solution at the fixed point is: $\bar{V}_2 = 125.18$ V, $\bar{\delta}_2 = -0.0275$ rad. The matrix $[\partial V/\partial \hat{Q}]$ is just a scalar, and can be evaluated from (17):

$$\begin{aligned} \frac{\partial V_2}{\partial \hat{Q}_2} &= \left\{\frac{\partial Q_2}{\partial V_2} - \left(\frac{\partial Q_2}{\partial \delta_2}\right)\left(\frac{\partial P_2}{\partial \delta_2}\right)^{-1}\left(\frac{\partial P_2}{\partial V_2}\right)\right\}^{-1} \\ &= 0.00219\ \frac{\text{V}}{\text{VAr}}. \end{aligned} \tag{19}$$

According to (6), the Jacobian matrix evaluates to:

$$J = \begin{cases} -2.448 & \text{for a Type-A system} \\ 0.655 & \text{for a Type-B system.} \end{cases} \tag{20}$$

The Jacobian $J$ is a scalar, so its eigenvalue is the same number. Therefore, the Type-A system is unstable, whereas the Type-B system is locally asymptotically stable.

*2) Stability of Three-Bus Example:* The three-bus example is a two-dimensional discrete-time system, with stationary state $\bar{Q} = [-318.16 \quad -132.82]^T$ VAr. Both points correspond to the fourth segment of the droop control function (between $V^c$ and $V^d$), so $\partial q_2/\partial V_2 = \partial q_3/\partial V_3 = -1118$ VAr/V. The fixed point steady-state voltage magnitudes and angles are: $\bar{V}_2 = 125.28$ V, $\bar{\delta}_2 = -0.0097$ rad, $\bar{V}_3 = 125.12$ V, and $\bar{\delta}_3 = -0.0103$ rad. Using (17), one may obtain

$$\left[\frac{\partial V}{\partial \hat{Q}}\right] = \begin{bmatrix} 0.002196 & 0.002201 \\ 0.002199 & 0.002418 \end{bmatrix}\ \frac{\text{V}}{\text{VAr}}\,. \tag{21}$$

The Jacobian matrix (6) of the Type-A system is

$$J = \begin{bmatrix} -2.4552 & -2.4608 \\ -2.4586 & -2.7034 \end{bmatrix} \tag{22}$$

with eigenvalues $\lambda_1 = -0.116$ and $\lambda_2 = -5.042$. Hence, the Type-A system is unstable. On the other hand, the Jacobian matrix of the Type-B system is

$$J = \begin{bmatrix} 0.6545 & -0.2461 \\ -0.2459 & 0.6297 \end{bmatrix} \tag{23}$$

with eigenvalues $\mu_1 = 0.888$ and $\mu_2 = 0.396$, which can alternatively be obtained by applying (10). Hence, the Type-B system is locally asymptotically stable.

## III. Case Studies

This section contains a distillation of results from extensive simulation studies on a wide range of distribution feeders that were modeled in very high detail. Our findings indicate that the proposed voltage controller with appropriate parameter settings would successfully control the voltages within normal bounds in all cases.

### A. Modeling of Rooftop PV Panels

The incident solar radiation on a tilted PV array is calculated using classical formulas [24], implemented in GridLAB-D. The calculation involves various types of irradiance adjusted for time of day, the site latitude, and the orientation and tilt angle of the PV panels.

In the simulations, PV panels are virtually installed on residential rooftops according to a PV penetration level parameter, which is defined as

$$\text{penetration level} = \frac{\text{residential customers with PV systems}}{\text{total number of residential customers in the feeder}}. \tag{24}$$

The houses are assumed to have two types of orientation, namely, north-south and east-west. The orientation of houses with PV systems is split in a 3:1 ratio, signifying that there is higher probability that PV panels will be installed on a south-facing rather than on a west-facing roof in the northern hemisphere. The roof angle is uniformly selected from a set with pitch equal to $x/12$, where $x = \{0, 3, 4, \ldots, 12\}$. If the roof is flat ($x = 0$), the solar panels are assumed to be facing south and tilted to a degree equal to the site latitude; otherwise, solar panels are assumed to be installed parallel to the roof.

The southern or western part of the roof area is set equal to $(0.5) \cdot (\text{floor area})/\cos(\text{roof angle})$. Then the total panel area is randomly generated according to a uniform distribution within 50% to 90% of the south- or west-facing roof area. For a given PV panel area value, the nominal apparent power rating of the inverter should satisfy

$$\begin{aligned} S^{\max} &\geq (\text{CF}) \cdot (\text{panel efficiency}) \\ &\quad \cdot (\text{rated insolation}) \cdot (\text{area}) \\ &= (1.15) \cdot (0.15) \\ &\quad \cdot \left(1000 \left(\frac{\text{W}}{\text{m}^2}\right)\right) \cdot (\text{area } (\text{m}^2)) \end{aligned} \tag{25}$$

where CF represents a corrective factor, since in certain cases the rated insolation can be exceeded. $S^{\max}$ is selected from a list that has been compiled from commercially available inverters (up to 30 kVA) [25], as the next higher value in the list. In other words, the most economical inverter that can handle the rated real power for any given PV installation is still being selected, so that additional investment costs for providing reactive power support are not incurred to the customer.[5]

Meteorological data are obtained from the National Renewable Energy Laboratory Measurement and Instrumentation Data Center (MIDC) database [26], which contains records of solar irradiance and air temperature recorded at 1-min intervals from several stations. Cloud effects are ignored, and all PV panels are assumed to receive the same amount of solar irradiance. A relatively temperate day with a sunny sky is selected (Feb. 27, 2011, from the Loyola Marymount University, University Hall, Los Angeles, CA, USA site). Light load conditions with high PV power production are most likely to cause undesirable voltage rise effects.

### B. Metrics for Evaluating Results

In this subsection, the metrics that are used to evaluate the performance of the proposed controller are described. The proposed metrics represent either extreme values or integrals of various time-varying quantities of interest, observed over a span of 24 h at a time interval of 60 s.

The first set of metrics is related to voltage. The voltage violation ratio (VVR) is defined as the maximum ratio of residential consumers with voltage limit violation (higher than 126 V or lower than 114 V). Ideally, VVR should be equal to zero, indicating no voltage violation throughout the day. Two other voltage-related metrics are the maximum and minimum voltage magnitudes ($V_{\max}$, $V_{\min}$) that appear at the meters of all residential consumers.

The second set of metrics is related to energy. These are the energy consumed by all loads ($E_{\text{load}}$), the energy losses of the network ($E_{\text{loss}}$), the energy generated by all PV systems ($E_{\text{PV}}$), and the energy measured at the substation ($E_{\text{SS}}$). Also, by integrating reactive power, "reactive energy" metrics can be defined, measured in MVAr-h. These are the reactive energy measured at the substation ($E^Q_{\text{SS}}$) and the reactive energy generated by all PV systems ($E^Q_{\text{PV}}$). The difference in an energy metric between the case where the PV inverters are actively regulating the voltage and the base (uncontrolled) case is denoted by "$\Delta E$."

In general, we expect to obtain negative values for $\Delta E^Q_{\text{PV}}$, whereas typically positive $\Delta E_{\text{loss}}$ and $\Delta E^Q_{\text{SS}}$ represent increased real and reactive energy losses throughout the distribution feeder. $\Delta E_{\text{PV}}$ should be negative because of extra inverter losses due to the reactive power current component. Also, since the voltages are decreased, this usually results in lower power consumption (from voltage-dependent loads) thus yielding negative values of $\Delta E_{\text{load}}$. Finally, it is interesting to note that the change in substation energy $\Delta E_{\text{SS}}$ can be either positive or negative. This is because $\Delta E_{\text{SS}} = \Delta E_{\text{load}} + \Delta E_{\text{loss}} + (-\Delta E_{\text{PV}})$, is determined by the sum of quantities of different sign (negative, positive, and positive, respectively).

In the simulations, the real power loss of the inverter is modeled as a linear function of its apparent power:

$$P^{\text{inv}}_n = \hat{P}_n - (0.04)\sqrt{(\hat{P}_n)^2 + (\hat{Q}_n)^2}\,. \tag{26}$$

[5]The additional functionality of reactive power support should not increase the cost of inverters significantly. Any standard inverter can be made to absorb/supply reactive power, with only slight modifications in its controller code, and with exactly the same power electronics circuit as before.

### C. Distribution Feeders

This subsection provides some details about the distribution systems that are used for the case studies. The houses are virtually equipped with rooftop PV systems using the method described above at various penetration levels. All feeders are connected to a high-voltage bus through a substation transformer with an impedance of $0.009 + j0.06$ pu. Voltage regulators are deactivated. The voltage at the transmission side of the substation transformer for all feeders is assumed to be constant and equal to 1.05 pu, except for feeders R1–1247-2 and R1–2500-1, where it is 1.04 pu, and feeder R5–1247-3, where it is 1.02 pu.

*1) Agent-Based Distribution Test Feeder:* A so-called "agent-based distribution test feeder" (ABDTF) has been developed by the authors [27], based on an actual feeder of an electric utility in Iowa, with detailed specifications for feeder equipment (such as fuses, switches, overhead and underground conductors, and service transformers) as well as for residential and/or commercial customers, including the floor areas of the houses.[6] Fig. 6 depicts a schematic of the topology of the feeder that includes all branches at the medium-voltage level. Exact geographic coordinates of its components are also known, but are not reflected in the figure. The peak power of the feeder at the substation is reported by the utility to be approximately 14 MVA, and the primary distribution voltage is 13.2 kV. The end-use loads of the households include conventional thermostatically controlled air-conditioning, water heaters, TV sets, fans, lights, ovens, and other common electric devices. This feeder has 1372 houses.

*2) PNNL Taxonomy Feeders:* The so-called "taxonomy feeders" are prototypical feeders developed by researchers at PNNL. They represent the fundamental characteristics of radial distribution feeders found in the U.S., based on 575 distribution feeders from 151 separate substations from different utilities across the U.S. Each prototypical feeder is characterized as belonging to one of five U.S. climate regions,[7] by primary distribution voltage level, and other features [28], [29]. The models of the taxonomy feeders are provided as part of the GridLAB-D software package. Simulation studies were performed on all 22 taxonomy feeders that contain houses. The feeders have been modeled with high fidelity from the substation down to the individual customer meters, including detailed end-use load representations (heating, ventilation, and air-conditioning, and various other constant impedance, current, and power loads). Floor areas are provided as part of the model parameters.

### D. Simulation Results

In the studies described below, the "no droop" case represents a base scenario where none of the inverters is regulating the voltage, whereas in the "all droop" case all inverters are regulating their local voltage, and have the same droop function parameters. The inverters are distributed in a random fashion around the distribution feeder. In the simulations, Volt/VAr support is not active overnight. It is activated in the morning, as soon as real PV power generation begins, and deactivated at sunset.

[6]In its original implementation, the feeder was equipped with an array of intelligent "agents," such as price-responsive air-conditioning units and plug-in electric vehicles, hence the name of the feeder. However, this type of functionality has now been disabled, and the feeder only contains conventional non-price-responsive load.

[7]Region 1 is the U.S. west coast, region 2 is the north-central and eastern U.S., region 3 is the non-coastal southwest U.S., region 4 is the non-coastal southeast and central U.S., and region 5 is the southeast.

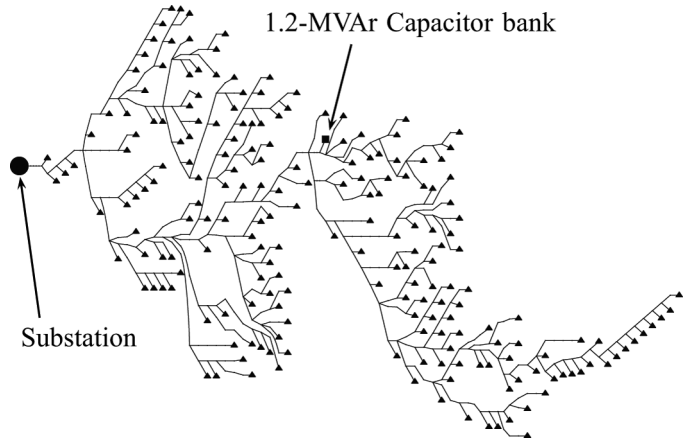


Fig. 6. Schematic of the feeder topology (this is not an accurate geographic representation). The triangles at the leaves of this tree represent distribution transformers.

TABLE I
ABDTF METRICS FOR 15% AND 30% PENETRATION LEVEL

| Metrics | 15% No droop | 15% All droop | 30% No droop | 30% All droop |
|---|---|---|---|---|
| $D$ (V) | N/A | 10 | N/A | 10 |
| VVR (%) | 5.32 | 0.00 | 47.52 | 0.00 |
| $V_{\max}$ (V) | 126.63 | 125.86 | 127.11 | 125.88 |
| $V_{\min}$ (V) | 120.58 | 120.57 | 120.33 | 120.34 |
| $\Delta E_{\text{load}}$ (MWh) | 50.505* | −0.0127 | 51.027* | −0.033 |
| $\Delta E_{\text{loss}}$ (MWh) | 0.928* | 0.007 | 0.909* | 0.021 |
| $\Delta E_{\text{PV}}$ (MWh) | 9.369* | −0.008 | 17.286* | −0.023 |
| $\Delta E_{\text{SS}}$ (MWh) | 42.063* | 0.003 | 34.650* | 0.010 |
| $\Delta E^{Q}_{\text{SS}}$ (MVAr-h) | 16.460* | 1.402 | 16.514* | 3.474 |
| $\Delta E^{Q}_{\text{PV}}$ (MVAr-h) | 0.000* | −1.398 | 0.000* | −3.457 |

* These values represent energies for the base case.

TABLE II
ABDTF METRICS FOR 50% PENETRATION LEVEL

| $D$ (V) | VVR (%) | $V_{\max}$ (V) | $V_{\min}$ (V) | $\Delta E_{\text{load}}$ (MWh) | $\Delta E_{\text{loss}}$ (MWh) | $\Delta E_{\text{PV}}$ (MWh) | $\Delta E_{\text{SS}}$ (MWh) | $\Delta E^{Q}_{\text{SS}}$ (MVAr-h) | $\Delta E^{Q}_{\text{PV}}$ (MVAr-h) |
|---|---|---|---|---|---|---|---|---|---|
| N/A | 94.1 | 128.8 | 120.8 | 50.40* | 0.94* | 30.73* | 20.62* | 16.46* | 0.00* |
| 10 | 0.0 | 125.9 | 120.8 | −0.080 | 0.056 | −0.051 | 0.027 | 7.677 | −7.623 |
| 9 | 0.0 | 125.9 | 120.8 | −0.110 | 0.079 | −0.086 | 0.055 | 10.369 | −10.291 |
| 8 | 0.0 | 125.9 | 120.8 | −0.127 | 0.106 | −0.130 | 0.109 | 13.049 | −12.942 |
| 7 | 0.0 | 125.9 | 120.8 | −0.162 | 0.135 | −0.179 | 0.152 | 15.572 | −15.432 |
| 6 | 0.0 | 125.9 | 120.8 | −0.176 | 0.165 | −0.230 | 0.218 | 17.886 | −17.711 |
| 5 | 0.0 | 125.9 | 120.6 | −0.200 | 0.195 | −0.279 | 0.274 | 19.993 | −19.783 |
| 4 | 0.0 | 125.9 | 120.4 | −0.230 | 0.225 | −0.327 | 0.321 | 21.907 | −21.660 |
| 3 | 0.0 | 125.9 | 120.3 | −0.237 | 0.254 | −0.372 | 0.389 | 23.650 | −23.366 |
| 2 | 0.0 | 125.9 | 120.1 | −0.250 | 0.283 | −0.415 | 0.448 | 25.246 | −24.926 |
| 1 | 0.0 | 125.9 | 119.8 | −0.276 | 0.311 | −0.455 | 0.489 | 26.713 | −26.357 |

* These values represent energies for the base case.

*1) ABDTF:* Studies are first run for two different penetration levels (15% and 30%), with constant droop function parameters ($V^a = 114$ V, $D = 10$ V, and $V^d = 126$ V). Table I contains the simulation metrics for these studies. Then studies are conducted for a 50% penetration level, with varying droop function parameters (same $V^a$, $V^d$ as before, but different $D$). Table II summarizes these simulation results.

*15% Penetration Level:* For this case, 231 houses are assumed to have PV systems. The maximum uncontrolled voltage ($V_{\max} = 126.63$ V) is higher than 126 V, and causes the absorp-

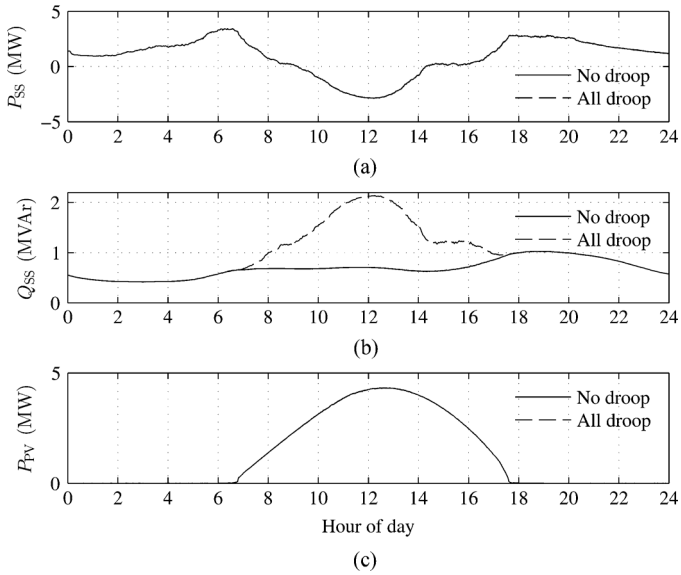


Fig. 7. 50% PV penetration in ABDTF: (a) real power at the substation; (b) reactive power at the substation; (c) total PV real power generation.

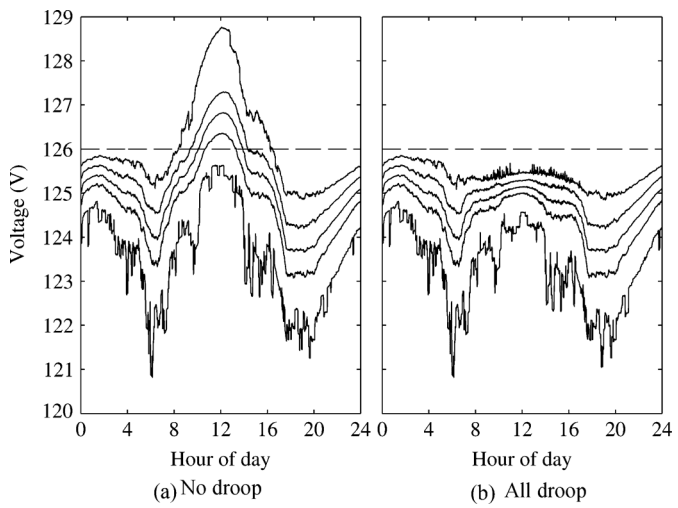


Fig. 8. Statistics of voltages at meters of residential loads for 50% PV penetration in ABDTF ($V^a = 114$ V, $V^d = 126$ V, $D = 10$ V). The five traces correspond to the minimum, mean value minus one standard deviation, mean value, mean value plus one standard deviation, and maximum voltage.

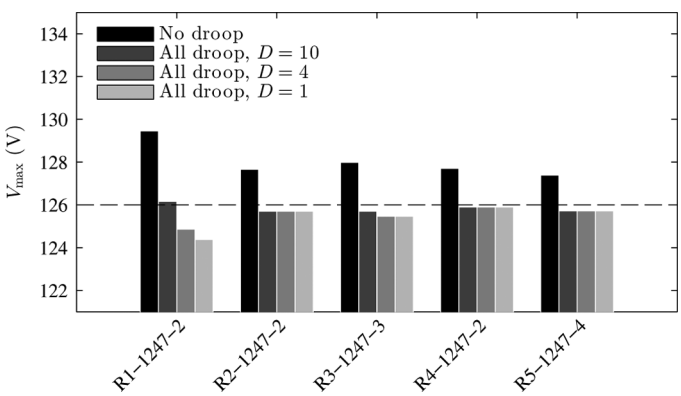


Fig. 9. Maximum voltage in PNNL taxonomy feeders for 50% penetration level.

tion of a minor amount of reactive power in the controlled case ($E^Q_{\rm PV} = -1.398$ MVAr-h). The voltages in the controlled case are in compliance with ANSI Standard C84.1.

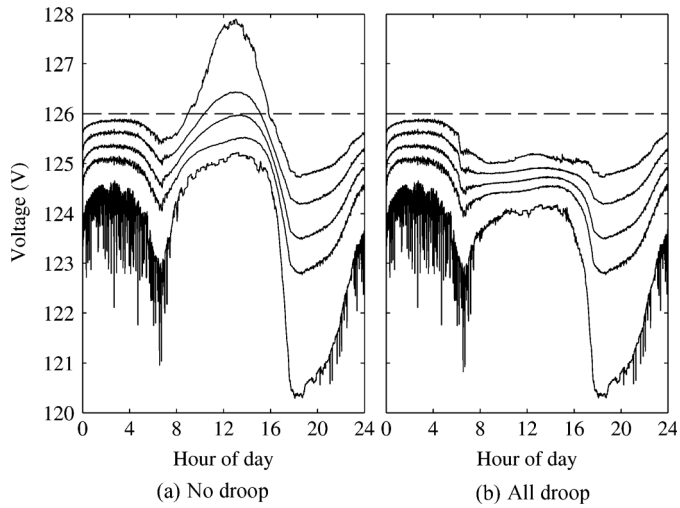


Fig. 10. Statistics of voltages at meters of residential loads for 50% PV penetration in PNNL feeder R5–3500-1 ($V^a = 114$ V, $V^d = 126$ V, $D = 10$ V).

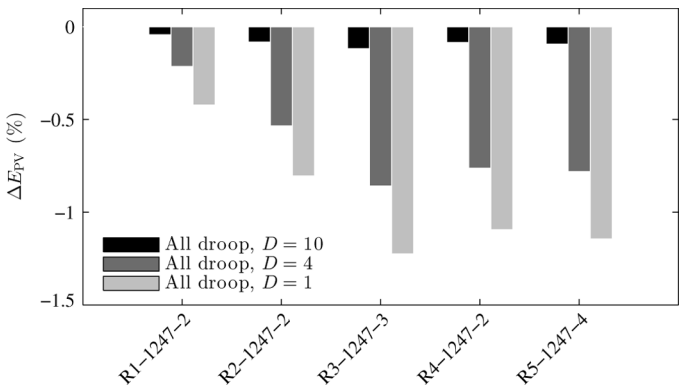


Fig. 11. Relative change of PV energy in PNNL taxonomy feeders for 50% penetration level.

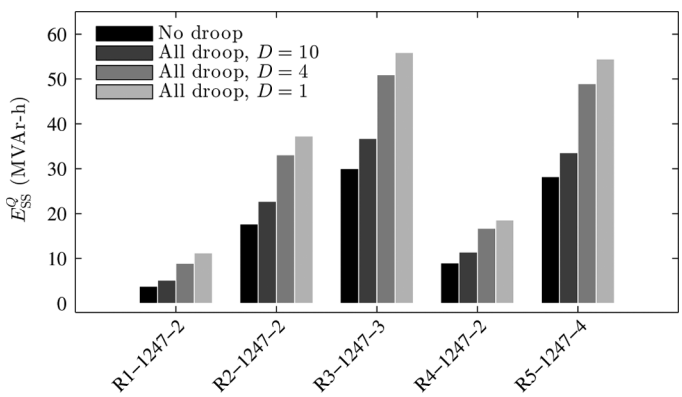


Fig. 12. Reactive energy at the substation in PNNL taxonomy feeders for 50% penetration level.

*30% Penetration Level:* In this case, 433 houses are assumed to have PV systems. In the uncontrolled case, almost 50% of residential customers experience an overvoltage at some point in the day. However, the voltage controllers successfully mitigate this issue.

*50% Penetration Level:* For this case, 733 houses are assumed to have PV units. As can be observed in Fig. 7(a), the real power flow at the substation is reversed during the daytime. Fig. 7(b) reflects the level of reactive power absorbed from the

TABLE III
PNNL TAXONOMY FEEDER METRICS FOR 50% PENETRATION LEVEL

| $D$ (V) | VVR (%) | $V_{max}$ (V) | $V_{min}$ (V) | $\Delta E_{load}$ (MWh) | $\Delta E_{loss}$ (MWh) | $\Delta E_{PV}$ (MWh) | $\Delta E_{SS}$ (MWh) | $\Delta E^{Q}_{SS}$ (MVAr-h) | $\Delta E^{Q}_{PV}$ (MVAr-h) |
|---|---|---|---|---|---|---|---|---|---|
| R1-1247-1 with 1594 houses and 777 PV systems | | | | | | | | | |
| N/A | 43.9 | 129.52 | 114.33 | 63.06* | 1.85* | 46.70* | 18.21* | 22.47* | 0.00* |
| 10.00 | 0.19 | 126.92 | 114.30 | −0.073 | 0.045 | −0.010 | −0.019 | 3.271 | −3.175 |
| 4.00 | 0.00 | 125.99 | 114.30 | −0.288 | 0.168 | −0.105 | −0.014 | 13.299 | −12.919 |
| 1.00 | 0.00 | 125.99 | 114.27 | −0.412 | 0.250 | −0.183 | 0.022 | 18.193 | −17.627 |
| R1-1247-2 with 544 houses and 286 PV systems | | | | | | | | | |
| N/A | 39.3 | 129.46 | 114.82 | 22.87* | 0.84* | 17.32* | 6.39* | 3.80* | 0.00* |
| 10.00 | 0.18 | 126.17 | 114.82 | −0.020 | 0.025 | −0.007 | 0.012 | 1.353 | −1.318 |
| 4.00 | 0.00 | 124.87 | 114.80 | −0.081 | 0.081 | −0.037 | 0.037 | 5.145 | −5.021 |
| 1.00 | 0.00 | 124.38 | 114.26 | −0.117 | 0.122 | −0.073 | 0.078 | 7.435 | −7.253 |
| R1-1247-3 with 22 houses and 12 PV systems | | | | | | | | | |
| N/A | 100.0 | 126.20 | 123.42 | 10.33* | 0.05* | 0.73* | 9.66* | 0.54* | 0.00* |
| 10.00 | 0.00 | 125.73 | 123.42 | −0.007 | 0.002 | −0.003 | −0.002 | 0.319 | −0.319 |
| 4.00 | 0.00 | 125.73 | 122.34 | −0.015 | 0.008 | −0.014 | 0.006 | 0.731 | −0.729 |
| 1.00 | 0.00 | 125.73 | 121.94 | −0.018 | 0.010 | −0.017 | 0.009 | 0.828 | −0.824 |
| R1-1247-4 with 652 houses and 339 PV systems | | | | | | | | | |
| N/A | 56.4 | 130.04 | 116.35 | 45.54* | 0.68* | 21.37* | 24.86* | 19.54* | 0.00* |
| 10.00 | 0.61 | 126.67 | 116.35 | −0.067 | 0.053 | −0.014 | −0.000 | 3.008 | −2.968 |
| 4.00 | 0.00 | 124.88 | 116.35 | −0.212 | 0.176 | −0.090 | 0.054 | 9.215 | −9.071 |
| 1.00 | 0.00 | 124.88 | 116.25 | −0.276 | 0.249 | −0.149 | 0.122 | 12.033 | −11.816 |
| R1-2500-1 with 40 houses and 21 PV systems | | | | | | | | | |
| N/A | 2.5 | 126.14 | 122.39 | 19.50* | 0.31* | 1.34* | 18.47* | −10.35* | 0.00* |
| 10.00 | 0.00 | 125.88 | 122.38 | −0.001 | −0.000 | −0.002 | 0.000 | 0.146 | −0.145 |
| 4.00 | 0.00 | 125.88 | 122.34 | −0.004 | −0.002 | −0.018 | 0.011 | 1.020 | −1.022 |
| 1.00 | 0.00 | 125.88 | 121.96 | −0.006 | −0.001 | −0.025 | 0.017 | 1.286 | −1.288 |
| R2-1247-1 with 176 houses and 87 PV systems | | | | | | | | | |
| N/A | 15.3 | 126.57 | 123.96 | 49.80* | 0.59* | 6.94* | 43.46* | 5.21* | 0.00* |
| 10.00 | 0.00 | 125.99 | 123.96 | −0.043 | 0.005 | −0.023 | −0.015 | 2.178 | −2.171 |
| 4.00 | 0.00 | 125.99 | 122.61 | −0.140 | 0.029 | −0.132 | 0.022 | 6.811 | −6.760 |
| 1.00 | 0.00 | 125.99 | 121.94 | −0.162 | 0.039 | −0.164 | 0.041 | 7.897 | −7.829 |
| R2-1247-2 with 836 houses and 437 PV systems | | | | | | | | | |
| N/A | 82.7 | 127.66 | 120.38 | 40.73* | 0.93* | 33.67* | 7.99* | 17.67* | 0.00* |
| 10.00 | 0.00 | 125.70 | 120.38 | −0.090 | 0.043 | −0.028 | −0.019 | 5.071 | −5.023 |
| 4.00 | 0.00 | 125.70 | 119.94 | −0.284 | 0.152 | −0.180 | 0.048 | 15.443 | −15.219 |
| 1.00 | 0.00 | 125.70 | 118.91 | −0.360 | 0.215 | −0.271 | 0.126 | 19.640 | −19.299 |
| R2-1247-3 with 1506 houses and 756 PV systems | | | | | | | | | |
| N/A | 24.5 | 128.86 | 114.11 | 60.47* | 1.68* | 49.83* | 12.33* | 25.09* | 0.00* |
| 10.00 | 0.07 | 126.70 | 114.09 | −0.029 | 0.005 | −0.004 | −0.020 | 1.306 | −1.272 |
| 4.00 | 0.00 | 125.91 | 114.10 | −0.204 | 0.040 | −0.051 | −0.114 | 7.776 | −7.661 |
| 1.00 | 0.00 | 125.91 | 114.14 | −0.331 | 0.073 | −0.102 | −0.157 | 12.032 | −11.874 |
| R2-2500-1 with 910 houses and 465 PV systems | | | | | | | | | |
| N/A | 43.8 | 127.11 | 121.95 | 142.72* | 1.35* | 38.06* | 106.01* | 24.25* | 0.00* |
| 10.00 | 0.00 | 125.98 | 121.81 | −0.203 | 0.056 | −0.072 | −0.074 | 9.632 | −9.582 |
| 4.00 | 0.00 | 125.98 | 120.99 | −0.627 | 0.236 | −0.500 | 0.109 | 29.981 | −29.702 |
| 1.00 | 0.00 | 125.98 | 120.52 | −0.759 | 0.316 | −0.664 | 0.222 | 35.873 | −35.482 |
| R2-3500-1 with 90 houses and 44 PV systems | | | | | | | | | |
| N/A | 13.3 | 126.13 | 123.67 | 94.62* | 0.77* | 3.17* | 92.22* | 0.61* | 0.00* |
| 10.00 | 0.00 | 125.97 | 123.66 | −0.014 | 0.000 | −0.014 | −0.000 | 0.795 | −0.788 |
| 4.00 | 0.00 | 125.93 | 123.14 | −0.092 | 0.010 | −0.085 | 0.003 | 3.846 | −3.818 |
| 1.00 | 0.00 | 125.93 | 122.89 | −0.106 | 0.014 | −0.101 | 0.009 | 4.393 | −4.359 |
| R3-1247-1 with 457 houses and 232 PV systems | | | | | | | | | |
| N/A | 5.3 | 126.26 | 123.81 | 62.95* | 1.26* | 12.51* | 51.69* | 13.86* | 0.00* |
| 10.00 | 0.00 | 125.94 | 123.76 | −0.071 | 0.008 | −0.031 | −0.033 | 3.567 | −3.558 |
| 4.00 | 0.00 | 125.94 | 122.66 | −0.248 | 0.054 | −0.243 | 0.049 | 12.499 | −12.416 |
| 1.00 | 0.00 | 125.94 | 122.14 | −0.285 | 0.072 | −0.306 | 0.093 | 14.600 | −14.486 |
| R3-1247-3 with 1326 houses and 725 PV systems | | | | | | | | | |
| N/A | 64.4 | 127.98 | 120.51 | 50.48* | 2.75* | 33.89* | 19.34* | 30.05* | 0.00* |
| 10.00 | 0.00 | 125.70 | 120.50 | −0.080 | 0.046 | −0.040 | 0.007 | 6.724 | −6.699 |
| 4.00 | 0.00 | 125.47 | 119.61 | −0.263 | 0.182 | −0.291 | 0.211 | 20.897 | −20.742 |
| 1.00 | 0.00 | 125.47 | 118.96 | −0.326 | 0.259 | −0.415 | 0.348 | 25.861 | −25.619 |
| R4-1247-1 with 523 houses and 239 PV systems | | | | | | | | | |
| N/A | 14.7 | 126.99 | 120.05 | 32.49* | 1.04* | 17.80* | 15.73* | 18.35* | 0.00* |
| 10.00 | 0.00 | 125.73 | 120.06 | −0.047 | 0.009 | −0.017 | −0.020 | 3.066 | −3.062 |
| 4.00 | 0.00 | 125.56 | 119.28 | −0.174 | 0.063 | −0.183 | 0.072 | 11.869 | −11.793 |
| 1.00 | 0.00 | 125.56 | 119.25 | −0.217 | 0.090 | −0.255 | 0.129 | 14.651 | −14.528 |
| R4-1247-2 with 370 houses and 212 PV systems | | | | | | | | | |
| N/A | 87.0 | 127.70 | 120.45 | 14.09* | 0.49* | 13.77* | 0.82* | 8.99* | 0.00* |
| 10.00 | 0.00 | 125.90 | 120.43 | −0.028 | 0.007 | −0.012 | −0.009 | 2.425 | −2.423 |
| 4.00 | 0.00 | 125.90 | 118.56 | −0.095 | 0.034 | −0.105 | 0.045 | 7.722 | −7.697 |
| 1.00 | 0.00 | 125.90 | 117.68 | −0.118 | 0.049 | −0.151 | 0.081 | 9.577 | −9.533 |
| R4-2500-1 with 168 houses and 72 PV systems | | | | | | | | | |
| N/A | 16.1 | 127.39 | 118.87 | 5.92* | 0.22* | 4.80* | 1.34* | 4.05* | 0.00* |
| 10.00 | 0.00 | 125.96 | 118.88 | −0.007 | 0.003 | −0.004 | 0.000 | 0.583 | −0.581 |
| 4.00 | 0.00 | 125.96 | 118.88 | −0.027 | 0.010 | −0.023 | 0.006 | 1.911 | −1.904 |
| 1.00 | 0.00 | 125.96 | 118.00 | −0.037 | 0.014 | −0.035 | 0.012 | 2.491 | −2.480 |
| R5-1247-1 with 1002 houses and 536 PV systems | | | | | | | | | |
| N/A | 9.1 | 126.86 | 120.07 | 77.91* | 1.01* | 38.48* | 40.44* | 24.89* | 0.00* |
| 10.00 | 0.00 | 125.31 | 120.07 | −0.057 | 0.011 | −0.007 | −0.039 | 2.375 | −2.359 |
| 4.00 | 0.00 | 125.31 | 120.08 | −0.399 | 0.103 | −0.213 | −0.083 | 17.779 | −17.597 |
| 1.00 | 0.00 | 125.31 | 118.99 | −0.549 | 0.160 | −0.346 | −0.044 | 23.733 | −23.431 |
| R5-1247-2 with 306 houses and 172 PV systems | | | | | | | | | |
| N/A | 6.2 | 128.27 | 115.67 | 40.44* | 0.64* | 11.98* | 29.11* | 19.39* | 0.00* |
| 10.00 | 0.33 | 126.43 | 115.67 | −0.019 | 0.010 | −0.004 | −0.005 | 0.797 | −0.793 |
| 4.00 | 0.00 | 125.66 | 115.56 | −0.162 | 0.102 | −0.095 | 0.035 | 6.709 | −6.659 |
| 1.00 | 0.00 | 125.66 | 115.61 | −0.217 | 0.149 | −0.147 | 0.080 | 8.871 | −8.786 |
| R5-1247-3 with 2024 houses and 1065 PV systems | | | | | | | | | |
| N/A | 46.5 | 134.31 | 114.23 | 68.72* | 4.18* | 73.83* | −0.93* | 13.65* | 0.00* |
| 10.00 | 10.13 | 127.91 | 114.19 | −0.244 | 0.084 | −0.039 | −0.121 | 7.093 | −6.392 |
| 4.00 | 0.00 | 125.98 | 114.23 | −0.451 | 0.167 | −0.064 | −0.220 | 11.651 | −10.520 |
| 1.00 | 0.00 | 125.90 | 114.23 | −0.559 | 0.258 | −0.115 | −0.185 | 15.270 | −13.790 |
| R5-1247-4 with 926 houses and 493 PV systems | | | | | | | | | |
| N/A | 39.6 | 127.39 | 121.32 | 60.59* | 1.27* | 36.77* | 25.09* | 28.20* | 0.00* |
| 10.00 | 0.00 | 125.71 | 121.27 | −0.096 | 0.038 | −0.034 | −0.024 | 5.349 | −5.344 |
| 4.00 | 0.00 | 125.71 | 120.70 | −0.385 | 0.188 | −0.287 | 0.090 | 20.778 | −20.696 |
| 1.00 | 0.00 | 125.71 | 119.73 | −0.485 | 0.269 | −0.421 | 0.204 | 26.263 | −26.115 |
| R5-1247-5 with 1539 houses and 802 PV systems | | | | | | | | | |
| N/A | 35.7 | 128.78 | 117.90 | 70.80* | 2.10* | 59.59* | 13.31* | 37.42* | 0.00* |
| 10.00 | 0.06 | 126.04 | 118.02 | −0.127 | 0.079 | −0.026 | −0.023 | 4.857 | −4.765 |
| 4.00 | 0.00 | 125.79 | 117.57 | −0.489 | 0.263 | −0.177 | −0.049 | 19.254 | −18.837 |
| 1.00 | 0.00 | 125.79 | 117.78 | −0.671 | 0.382 | −0.292 | 0.003 | 25.898 | −25.245 |
| R5-2500-1 with 2146 houses and 1095 PV systems | | | | | | | | | |
| N/A | 30.8 | 130.40 | 115.57 | 96.91* | 1.99* | 88.83* | 10.07* | 51.49* | 0.00* |
| 10.00 | 0.05 | 126.98 | 115.57 | −0.150 | 0.092 | −0.044 | −0.014 | 9.954 | −9.910 |
| 4.00 | 0.00 | 125.46 | 115.21 | −0.633 | 0.393 | −0.489 | 0.249 | 41.314 | −41.122 |
| 1.00 | 0.00 | 125.42 | 114.51 | −0.824 | 0.565 | −0.761 | 0.501 | 53.278 | −52.951 |
| R5-3500-1 with 2192 houses and 1155 PV systems | | | | | | | | | |
| N/A | 38.5 | 127.90 | 120.29 | 98.39* | 1.92* | 86.03* | 14.28* | 50.38* | 0.00* |
| 10.00 | 0.00 | 125.90 | 120.30 | −0.216 | 0.150 | −0.110 | 0.044 | 15.202 | −15.174 |
| 4.00 | 0.00 | 125.90 | 118.72 | −0.694 | 0.416 | −0.698 | 0.419 | 49.428 | −49.366 |
| 1.00 | 0.00 | 125.90 | 117.80 | −0.864 | 0.563 | −0.988 | 0.687 | 61.213 | −61.081 |

* These values represent energies for the base case.

PV inverters. Fig. 8 depicts the statistical distribution of voltages at the household meters. Fig. 8(a) illustrates that without the droop control the maximum voltages significantly exceed the upper limit for a substantial number of residential customers. Fig. 8(b) shows how the proposed controllers acting in unison can offset voltage rise conditions, and how all voltages remain below their upper limit. It can be observed that overvoltages have been mitigated in all controlled cases, but as $D$ decreases, reactive power absorption increases, which also increases the reactive energy at the substation and the total system loss.

*2) Taxonomy Feeders:* In the uncontrolled case, the voltage violation ratio (VVR) is always nonzero, as can be observed

from Table III of Appendix B. On the other hand, the proposed distributed control scheme mitigates overvoltages successfully in all cases (with the exception of a few cases where $D = 10$ V). Fig. 9 depicts the maximum voltage magnitudes that appear at the meters of all residential consumers for a selected subset of PNNL taxonomy feeders (one from each region). Fig. 10 illustrates the change in statistical distribution of voltages at the meters of the residential loads throughout the day in feeder R5–3500-1. Similar patterns are observed in all feeders. Generally, the estimated loss in PV energy production due to the reactive power control action is on the order of 1–2% (during this light-load day) as shown in Fig. 11 for the same five feeders as previously. Fig. 12 depicts the change in reactive energy consumption at the substation.

More comprehensive simulation results for all studies conducted on the 22 PNNL taxonomy feeders are given in Table III in Appendix B. It is noted that decreasing the deadband width $D$ is beneficial with respect to eliminating voltage rises. This could also improve the overall dynamic system stability, due to the corresponding reduction in the slope of the droop characteristic. However, it comes at the expense of higher inverter and distribution feeder energy loss, and substantially higher reactive power demand at the substation.

## IV. Conclusion

We studied the mitigation of voltage rise via reactive power absorption from distributed PV inverters. Analyses were conducted with detailed computer simulations of an array of real and realistic feeders representative of all U.S. regions for several PV penetration levels, as high as 50%. The results indicate that voltages can be successfully controlled within normal bounds in all cases that were analyzed.

In future work, it will be interesting to study the effect of cloud transients on distribution system performance using the proposed distributed Volt/VAr controller. One potential technical issue of high significance is the substantial amount of extra reactive power that is absorbed by the feeder at the substation. This reactive power would have to be compensated, perhaps using capacitor banks at the substation, otherwise problems related to transmission system voltage stability might arise. However, fast cloud transients and the reaction of the distributed Volt/VAr PV controllers might render capacitor bank-based compensation unsuitable for this purpose. Furthermore, it would be interesting to study if and how the proposed control scheme could be integrated into more conventional Volt/VAr controls that use capacitor banks and load tap changers.

## Appendix A
## Example System Parameters

The two-bus system has the following parameters: The voltage of bus 1 is fixed at $V_1 = 129$ V. The load consumes $P_l = 3$ kW and $Q_l = 1$ kVAr. The PV inverter is rated at $S^{\max} = 1.5$ kVA, and is assumed to be lossless. Its real power generation is initially zero, and is stepped to $P^{\text{inv}} = 1$ kW during period 6. The impedance of the line is $0.076 + j0.268\ \Omega$. The droop function parameters are $V^a = 114$ V, $V^d = 126$ V, and $D = 10$ V.

The three-bus system is similar to the two-bus system, with the following differences: The loads consume $P_{l2} = P_{l3} = 1.5$ kW and $Q_{l2} = Q_{l3} = 0.5$ kVAr. The line impedance between bus 1 and bus 2 is $0.076 + j0.268\ \Omega$, and the impedance between bus 2 and bus 3 is $0.0076 + j0.0268\ \Omega$.

## Appendix B
## Comprehensive Simulation Results for PNNL Taxonomy Feeders

Table III contains a comprehensive set of simulation results for studies conducted on 22 PNNL taxonomy feeders. The PV inverters are operating with various droop function parameters ($V^a = 114$ V, $V^d = 126$ V, variable $D$) under a 50% penetration level.

## References


[1] EPIA Market Report 2011, European Photovoltaic Industry Association (EPIA), Tech. Rep., Brussels, Belgium, 2011.

[2] T. A. Short, *Electric Power Distribution Handbook*. Boca Raton, FL, USA: CRC, 2003.

[3] M. H. Bollen and F. Hassan, *Integration of Distributed Generation in the Power System*. Hoboken, NJ, USA: Wiley, 2011.

[4] C. L. Masters, "Voltage rise: the big issue when connecting embedded generation to long 11 kV overhead lines," *Power Eng. J.*, vol. 16, no. 1, pp. 5–12, Feb. 2002.

[5] P. M. S. Carvalho, P. F. Correia, and L. A. F. Ferreira, "Distributed reactive power generation control for voltage rise mitigation in distribution networks," *IEEE Trans. Power Syst.*, vol. 23, no. 2, pp. 766–772, May 2008.

[6] M. Braun, T. Stetz, T. Reimann, B. Valov, and G. Arnold, "Optimal reactive power supply in distribution networks-technological and economic assessment for PV-systems," in *Proc. 24th Eur. Photov. Solar Energy Conf.*, Hamburg, Germany, Sep. 2009.

[7] L. Herman, B. Blazic, and I. Papic, "Voltage profile support in LV distribution networks with distributed generation," in *Proc. Univ. Power Eng. Conf. (UPEC)*, Glasgow, U.K., Sep. 2009, pp. 1–5.

[8] E. Demirok, D. Sera, R. Teodorescu, P. Rodriguez, and U. Borup, "Evaluation of the voltage support strategies for the low voltage grid connected PV generators," in *Proc. Energy Conv. Congr. Expo. (ECCE)*, Atlanta, GA, USA, Sep. 2010, pp. 710–717.

[9] M. Braun *et al.*, "Is the distribution grid ready to accept large-scale photovoltaic deployment? state of the art, progress, and future prospects," *Prog. Photovolt: Res. Appl.*, vol. 20, pp. 681–697, Nov. 2011.

[10] R. A. Shayani and M. A. G. De Oliveira, "Photovoltaic generation penetration limits in radial distribution systems," *IEEE Trans. Power Syst.*, vol. 26, no. 3, pp. 1625–1631, Aug. 2011.

[11] *American National Standard for Electric Power Systems and Equipment—Voltage Ratings (60 Hz)*, ANSI C84.1–2011 American National Standards Institute (ANSI) Std.

[12] M. E. Elkhatib, R. El-Shatshat, and M. M. A. Salama, "Novel coordinated voltage control for smart distribution networks with DG," *IEEE Trans. Smart Grid*, vol. 2, no. 4, pp. 598–605, Dec. 2011.

[13] Y. Ueda, K. Kurokawa, T. Tanabe, K. Kitamura, and H. Sugihara, "Analysis results of output power loss due to the grid voltage rise in grid-connected photovoltaic power generation systems," *IEEE Trans. Ind. Electron.*, vol. 55, no. 7, pp. 2744–2751, Jul. 2008.

[14] H. Kobayashi and H. Hatta, "Reactive power control method between DG using ICT for proper voltage control of utility distribution system," in *Proc. IEEE Power Energy Soc. General Meeting*, San Diego, CA, USA, Jul. 2011, pp. 1–6.

[15] R. Tonkoski and L. A. C. Lopes, "Impact of active power curtailment on overvoltage prevention and energy production of PV inverters connected to low voltage residential feeders," *Renew. Energy*, vol. 36, no. 12, pp. 3566–3574, Dec. 2011.

[16] M. Coddington, B. Kroposki, T. Basso, K. Lynn, C. Herig, and W. Bower, "High-penetration photovoltaic standards and codes workshop," in *Nat. Renewable Energy Lab.*, Denver, CO, USA, May 2010, Tech. Rep. NREL/TP-550–48378.

[17] M. H. J. Bollen and A. Sannino, "Voltage control with inverter-based distributed generation," *IEEE Trans. Power Del.*, vol. 20, no. 1, pp. 519–520, Jan. 2005.

[18] R. Neal and R. Bravo, "Advanced Volt/VAr control element of Southern California Edison's Irvine smart grid demonstration," in *Proc. IEEE Power Syst. Conf. Expo. (PSCE)*, Phoenix, AZ, USA, Mar. 2011, pp. 1–3.

[19] B. Bletterie *et al.*, "Development of innovative voltage control for distribution networks with high photovoltaic penetration," *Prog. Photovolt: Res. Appl.*, vol. 20, pp. 747–759, Nov. 2011.
[20] A. D. Domínguez-García and C. N. Hadjicostis, "Distributed algorithms for control of demand response and distributed energy resources," in *Proc. IEEE Control Decision Conf. (CDC-ECC)*, Orlando, FL, USA, Dec. 2011, pp. 27–32.
[21] Pacific Northwest National Laboratory (PNNL). [Online]. Available: http://www.gridlabd.org.
[22] K. Schneider, J. Fuller, F. Tuffner, and R. Singh, "Evaluation of conservation voltage reduction (CVR) on a national level," in *Pacific Northwest Nat. Laboratory (PNNL),* Tech. Rep., Richland, WA, USA, 2010.
[23] O. Galor*, Discrete Dynamical Systems*. Berlin, Germany: Springer, 2006.
[24] J. Duffie and W. Beckman*, Solar Energy Thermal Processes, Inc*. Hoboken, NJ, USA: Wiley, 1974.
[25] M. D. Martz, "Photon's annual inverter market survey," *Photon Mag.*, vol. 3, pp. 66–87, 2011.
[26] National Renewable Energy Laboratory, Measurement and Instrumentation Data Center. [Online]. Available: http://www.nrel.gov/midc/.
[27] P. Jahangiri, D. Wu, W. Li, D. C. Aliprantis, and L. Tesfatsion, "Development of an agent-based distribution test feeder with smart-grid functionality," in *Proc. IEEE Power Energy Soc. General Meeting*, San Diego, CA, USA, Jul. 2012.
[28] K. P. Schneider, Y. Chen, D. P. Chassin, R. Pratt, D. Engel, and S. Thompson, "Modern grid initiative distribution taxonomy final report," in *Pacific Northwest Nat. Lab., Tech. Rep*, Richland, WA, USA, Nov. 2008.
[29] K. P. Schneider, Y. Chen, D. Engle, and D. Chassin, "A taxonomy of North American radial distribution feeders," in *Proc. IEEE Power Energy Soc. General Meeting*, Calgary, AB, Canada, Jul. 2009.

**Pedram Jahangiri** (S'10) received the B.S. and M.S. degrees in electrical engineering from Isfahan University of Technology and Sharif University of Technology, Iran, in 2006 and 2008, respectively. He is currently working toward the Ph.D. degree in the Department of Electrical and Computer Engineering at Iowa State University, Ames, IA, USA, with research emphasis on smart distribution systems.

He was employed as an electrical engineering intern in the summer of 2012 by Energy Automation Solutions, Cooper Power Systems company, Minneapolis, MN, USA, where he worked on Volt/VAr management. He has been previously employed as a researcher by the Electric Ship Research and Development Consortium, Mississippi State University, MS, USA, and by the Automation of Complex Power Systems Center, RWTH University, Aachen, Germany.

**Dionysios C. Aliprantis** (SM'09) received the Diploma in electrical and computer engineering from the National Technical University of Athens, Greece, in 1999, and the Ph.D. from Purdue University, West Lafayette, IN, USA, in 2003.

He is currently an Assistant Professor of Electrical and Computer Engineering at Iowa State University, Ames, IA, USA. His research interests are related to electromechanical energy conversion and the analysis of power systems. More recently his work has focused on technologies that enable the integration of renewable energy sources in the electric power system, and the electrification of transportation.

Prof. Aliprantis was a recipient of the NSF CAREER award in 2009. He serves as an Associate Editor for the IEEE POWER ENGINEERING LETTERS and the IEEE TRANSACTIONS ON ENERGY CONVERSION.